

Supplementary Information

Redox-Copolymers for Nanofiltration-enabled Electrodialysis

Nayeong Kim,¹ Johannes Elbert,¹ Choonsoo Kim,² and Xiao Su^{1}*

¹ *Department of Chemical and Biomolecular Engineering, University of Illinois Urbana-Champaign, IL 61801, United States*

² *Department of Environmental Engineering with Institute of Energy/Environment Convergence Technologies and Department of Future Convergence Engineering, Kongju National University, 1223-24, Cheonan-daero, Cheonan-si 31080, Republic of Korea*

Corresponding Author

*E-mail: x2su@illinois.edu

Table of Contents

SI I. Experimental methods	3
SI II. Material synthesis	7
SI III. Electrochemical characterizations.....	16
SI IV. Performance of redox-polymer ED	19
SI V. Techno-economic analysis	29
References	34

SI I. Experimental methods

Materials

All chemicals were obtained from Sigma Aldrich, Fisher Scientific, TCI, or VWR, and used as received. 3-ferrocenylpropyl methacryl-amide (FPMAm) was synthesized as reported previously (**Figure S1**).¹ Cellulose-based dialysis membranes (Spectra/Por) were used as nanofiltration membranes, while anion- and cation-exchange membranes (CMVN, AMVN, Selemion) were used as ion-exchange membranes.

Chemical Characterization

To characterize the monomer ratio between FPMAm and METAC in P(FPMAm-co-METAC), ¹H-NMR spectra were recorded on a 500 MHz spectrometer with UI500NB. NMR sample was prepared with 10-15 mg of polymer in 700 μ L solvent. Polymer chain lengths were measured by GPC using the column of PSS NOVEMA Max (5 mm \times 50 mm \times 5 μ m) in 0.1 M NaCl and 0.1 vol% TFA. GPC was performed with respect to the Poly(2-vinylpyridine) standard with a sample volume of 50 μ L at a flow rate of 1 mL/min.

Liquid-phase analytics

The concentration of acetate (C2) was measured by Ion chromatography (IC, Dionex Integrion, Thermofisher Scientific) using an eluent concentration of 4.5 mM sodium bicarbonate and 1.4 mM sodium carbonate at the flow rate of 1.0 mL min⁻¹. The injection sample was prepared by 1:25 dilution with Deionized water (DI).

The concentrations of other carboxylates (from butyrate, C4 to decanoate, C10) were measured by RP-HPLC (Agilent 1260 Infinity II, Agilent) using the C₁₈ column (4.6 mm \times 100 mm \times 2.7 μ m, Agilent Poroshell 120). The elution gradient between phase A (0.1 vol% trifluoroacetic acid (TFA) in DI) and phase B (0.1 vol% TFA in MeOH) was used at a flow rate of 0.8 mL min⁻¹: 60% phase A for 0-4 min, 60-0% phase A for 4-14 min, 0-60% for 14-17 min, and 60% phase A for 17-19 min. The injection sample was prepared by 1:5 dilution with DI, and the injection volume was set to 50 μ L.

Carboxylates (C6-C10) in the redox channels were analyzed by LC-MS (LC/MSD iQ, Agilent). The C₁₈ column (2.1 mm \times 50 mm \times 2.7 μ m, Agilent Poroshell 120) was used with the same mobile phases as RP-HPLC and the following elution gradient at a flow rate of 0.4 mL min⁻¹: 50-0% phase A for 0-6 min, 0-50% phase A for 6-8 min, 50% phase A for 8-10 min. For both RP-HPLC and LC-MS, the concentrations of carboxylates were determined from the absorbance at a wavelength of 215 μ m. The injection sample was prepared by 1:5 dilution with phase A, and the injection volume was set to 30 μ L.

Electrochemical characterization

Cyclic voltammetry (CV) was performed at varying scan rates (100, 75, 50, 20, 10 mV s⁻¹) to verify the reversibility of the redox-copolymer and to calculate the diffusion coefficient (*D*). For CV, a three-electrode system, with Pt wires as working and counter electrodes and Ag/AgCl (3 M KCl) as a reference, was used

with the IR compensation. A solution containing 5 mL of 5 mM FPMAM in P(FPMAM₃₃-co-METAC₆₇) and 1 M NaCl was used as an electrolyte. Then, the D was calculated using the Randles-Sevcik equation (see *SI III. Electrochemical characterization* for details).

Rotating disc electrode (RDE) characterization was conducted to calculate the electron-transfer rate constants (k^0) at three different polymer chain lengths. A three-electrode system, with Pt disc (diameter=5 mm) as a working, carbon rod (diameter=5 mm) as a counter, and Ag/AgCl (3 M KCl) as a reference, was used. For RDE experiments, the rotation speed was varied from 400 to 1600 rpm. Then, applying the Koutecký-Levich equation and Tafel plot, electron-transfer rate constants were calculated. More detailed calculation methods can be found in *SI III. Electrochemical characterization*.

Electrochemical impedance spectroscopy (EIS) of the redox-polymer ED system was measured to calculate the membrane resistance (R_m) and charge transfer resistance (R_{ct}). EIS was performed in the frequency range of 10 mHz to 500 kHz at 0 V with an amplitude of 10 mV. The solution resistance (R_s), R_m , and R_{ct} were calculated based on an equivalent circuit of R(Q(RW)).

Linear sweep voltammetry (LSV) of the redox-polymer ED system was measured to compare the on-set potential of the redox reaction among different types of ED systems. To disregard the effects of adsorption, we ran LSV with bare Ti current collectors without carbon clothes electrodes. LSV was operated from 0 to 2 V at the scan rate of 1 mV s⁻¹.

Synthesis and characterization of P(FPMAM-co-METAC) (Pn)

A water-soluble redox-copolymer, P(FPMAM-co-METAC), was synthesized by free-radical copolymerization. An exemplary procedure for the synthesis of P(FPMAM-co-METAC) (P2) are following: FPMAM (2 g, 30 mol%), [2-(methacryloyloxy)ethyl]trimethyl-ammonium chloride (METAC, 3.902 mL, 70 mol%), and 4,4'-Azo-bis-(4-cyanovaleric acid) (ACVA, 300 mg, 5 mol%) were dissolved in methanol (25 mL). The mixture was degassed by bubbling with argon for 20 min and heated to 80 °C for 24 h. Then the polymer was dialyzed using a dialysis membrane with a molecular weight cut-off (MWCO) of 3,500 g mol⁻¹ against 500 mL of methanol twice. Next, the polymer was precipitated in 50 mL of diethyl ether and centrifuged. The polymer was redissolved in 2 mL of methanol, precipitated in diethyl ether, and centrifuged again. The centrifuged polymer was dried under vacuum conditions at 60 °C, with an 81% yield P(FPMAM-co-METAC).

The ratio between FPMAM and METAC was calculated by ¹H NMR (500 MHz, CDCl₃, δ): 4.1-4.7 (9 Hs, ferrocene) and 3.7-3.9 (2 Hs, methylene group from METAC) shown in **Figures S2-S5**. NMR analysis showed that P2 copolymer contains 33% FPMAM and 67% METAC, P(FPMAM₃₃-co-METAC₆₇). The polymer chain lengths were measured by gel permeation chromatography (GPC), shown in **Figures S7-S10**. Detailed descriptions of synthesis and polymer characterization can be found in *SI II. Material synthesis*.

Investigation of desalination performance and organic separation

The redox-polymer ED system was composed of cathode and anode compartments (redox channel (RC), $4 \times 4 \times 0.2 \text{ cm}^3$), the feed channel (FC, $4 \times 4 \times 0.5 \text{ cm}^3$), and the accumulating channel (AC, $4 \times 4 \times 0.5 \text{ cm}^3$). The descriptive configuration and assembly can be also found in Supplementary **Figure S14a** and previous papers.²

For parametric studies, 10 mM NaCl was used in both the FC and AC. Throughout the experiments, 20 mL of 30 mM P(FPMAm-co-METAC) was used as the redox-electrolyte and circulated in the RC, and activated carbon clothes (CH900-20, Kuraray) were used as electrodes ($3.5 \times 3.5 \text{ cm}^2$). We set the flow rates for all three channels to 5 mL min^{-1} . Unless it is mentioned, we operated the system for four hours at a constant voltage of 0.8 V. For carboxylate kinetics, 50 mL of 2 mM sodium acetate (C2), butyrate (C4), hexanoate (C6), octanoate (C8), and decanoate (C10) were used as treating water in the FC, while 50 mL of 10 mM NaCl was used in the AC. For desalination performance, the conductivity and pH were monitored by conductivity (3574-10C, Horiba) and pH meters (9615S-10D pH, Horiba). More descriptive experimental conditions and equations were elaborated in figure captions and *SI IV. Performance of redox-polymer ED*.

For a series of desalination (**Figures 4e and S22**), 20 mL of feed solutions of 10 mM, 100 mM, and 600 mM were semi-continuously flowing in the FC, while 20 mL of 10 mM NaCl was flowing semi-continuously in the AC at a flow rate of 5 mL/min. In the RC, 20 mL of 30 mM P(FPMAm-co-METAC) was used as the redox-electrolyte in circulation. While the feed solution and the AC solution were changing, the redox electrolyte, as well as the membranes were not changed. Then to demonstrate the cascade desalination of high-salinity source waters (100 mM and 600 mM) down to potable water salinity, the redox-copolymer was newly prepared.

To evaluate the desalination under the multi-component mixtures, we demonstrated wastewater desalination with a spike of 1 mM octanoate and 1 mM decanoate as representative of charged organic species (**Figure 4c**). Wastewater was collected from the Decatur wastewater treatment facility in Illinois after primary treatment with clarifiers. Semi-continuous of 20 mL wastewater were treated via our redox-polymer ED, and the performance was compared with the IEM-coupled redox-ED system. For IEM-coupled redox-ED, 20mL of 15 mM of ferricyanide and 15 mM of ferrocyanide were used as a redox-mediator in the RC. After the conductivity reached around $500 \mu\text{S/cm}$, we analyzed cation and anion composition in the FC, AC, and RC using IC, while organic species were analyzed by LC-MS. Also, to evaluate the distribution of organic species, we digested 2 cm X 2cm of electrodes and membranes in aqua regia for 24 hours and measured the concentration of organic species with LC-MS. In addition, attenuated total reflectance Fourier transforms infrared spectroscopy (ATR-FTIR, Cary 630 FTIR, Agilent) was monitored to investigate the membrane fouling in both redox-ED with IEM and redox-polymer ED with NF systems.

After use, redox polymers were recovered via the dialysis process using a dialysis membrane with MWCO of $3,500 \text{ g mol}^{-1}$ against 500 mL of DI twice and methanol once. We confirmed that the ratio of FPMAm and METAC for recycled P(FPMAm-co-METAC) was identical after the recovery process as shown in **Figure S6**. Thus, these recovered polymers were reused in a series of experiments.

To check the extent of polymer crossover in the FC and the AC, the iron concentration of the ferrocene unit was measured using inductively coupled plasma-optical emission spectrometry (ICP-OES) shown in **Tables S4-S7**.

Techno-economic Analysis

Assumptions were made to evaluate the economic feasibility of the redox-polymer ED based on TEA models developed for the ED system.^{3,4} In particular, we referred to mathematical models and performance metrics for major components of capital and operating costs, including stacking, auxiliary equipment, membrane replacement, and chemical costs (*SI V. Techno-economic analysis*).^{3,4}

The following assumptions were made: i) Both redox-polymer ED and conventional ED (IEM ED) treat 100 m³ of brackish water (1,200 μS) per day to potable water range (500 μS), operate 330 days a year, and conduct constant voltage operation. The large-scale systems are designed based on the desalination performance of our lab-scale system. Assuming both ED systems show comparable charge efficiencies, we calculated the operating voltage and energy consumption of IEM ED using linear sweep voltammetry (LSV) (**Figure S26a**). ii) We neglect pumping energy costs, assuming the energy for ED operation is much greater than the pump energy.⁴ And electricity cost was estimated based on the average cost of the United States \$0.11 kWh⁻¹. iii) We solely account for the upfront cost of the ED operation such as electricity, membranes, electrodes, and stacking costs, and set aside the cost of any pre-treatment and post-treatment processes. However, for redox-polymer ED, we added the cost for polymer synthesis in capital cost to account for the cost of the polymer material (**Table S9**). iv) We assumed systems are scaled up to 100 cm × 100 cm dimensions. Accounting for the previous studies by McGovern et al.⁴ and by Sajtar and Bagley,⁵ the equipment costs can be computed as 1,500 \$ m⁻² of membrane area. This assumption can be made for ED systems treating water volume up to 40,000 m³ per day and concentration of treating water under 7,000 ppm. v) To calculate unit water production cost (\$ m⁻³), we amortized the capital cost over 20 years. The major mathematical models can be found in *SI V. Techno-economic analysis* with detailed calculations, unit costs, and sources.

SI II. Material synthesis

Table S1 Summary of polymer sizes measured by gel permeation chromatography (GPC) with respect to the poly(2-vinylpyridine)

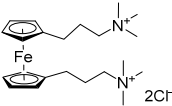
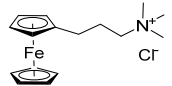
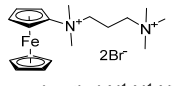
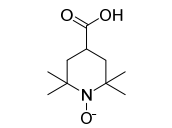
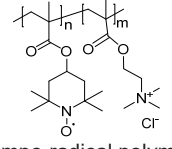
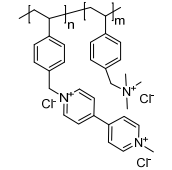
Polymer	Mn (g mol ⁻¹)	Mw (g mol ⁻¹)	Đ
P1	589	2,180	3.70
P2	1,480	10,700	7.23
P3	8,500	64,100	7.54
P2 (Large batch)	1,520	13,100	8.61

Table S2. Summary of P(FPMAm-co-METAC) synthesis and characteristic properties at varying polymer chain lengths

Polymer	ACVA [mol%]	Temperature [°C]	FPMAm content [%]	Yield [%]	E _{1/2} ^d [V]	D ^d [cm ² s ⁻¹]	k ₀ ^e [cm s ⁻¹]
P1 ^a	5	80	31	67	0.180	2.75×10 ⁻⁶	1.68×10 ⁻⁴
P2	5	80	33	81	0.205	2.38×10 ⁻⁶	2.16×10 ⁻³
P3	1	60	34	83	0.208	4.67×10 ⁻⁷	5.39×10 ⁻³

^{a)} 10 mol% of 2-mercaptoethanol was added as the chain-transfer agents; ^{b)} Analyzed by NMR; ^{c)} Determined by GPC in H₂O with 0.1 M NaCl + 0.1% trifluoroacetic acid and poly(2-vinylpyridine) calibration; ^{d)} Determined by CV (vs. Ag/AgCl in 3M KCl); ^{e)} Analyzed by RDE

Table S3 Summary of diffusion coefficient and electron-transfer constant of the P(FPMAm-co-METAC) and representative redox-active materials in aqueous electrolyte

Redox Active Material	Redox material / Electrolyte	Diffusion coefficient (cm ² s ⁻¹)	Electron-transfer constant (cm s ⁻¹)	ref
V ³⁺ / V ²⁺	50 mM / 1 M H ₂ SO ₄	2.4 × 10 ⁻⁶	5.3 × 10 ⁻⁴	6
VO ²⁺ / VO ₂ ⁺	50 mM / 1 M H ₂ SO ₄	3.9 × 10 ⁻⁶	8.5 × 10 ⁻⁴	6
[Fe(CN) ₆] ³⁻ / [Fe(CN) ₆] ⁴⁻	5 mM / 1 M KCl	7.26 ± 0.11 × 10 ⁻⁶	-	7
	10 mM / 1 M KCl	-	0.24	8
 Bis((3-trimethylammonio)propyl)Fc	1 mM / 0.5 M NaCl	3.1 × 10 ⁻⁶	1.4 × 10 ⁻²	9
 Ferrocenylmethyl trimethylammonium chloride	1.0 mM / 0.5 M NaCl	3.74 × 10 ⁻⁶	3.66 × 10 ⁻⁵	10
 N ¹ -ferrocenylmethyl-N ¹ ,N ¹ ,N ² ,N ² -pentamethylpropane-1,2-diaminium dibromide	1.0 mM / 0.5 M NaCl	3.64 × 10 ⁻⁶	4.60 × 10 ⁻⁶	10
 4-Carboxy-TEMPO	1 mM / 0.5 M KCl	2.64 × 10 ⁻⁶	2.25 × 10 ⁻³	11
 Tempo-radical polymer	2.5 mM / 0.1 M NaCl	7.0 ± 0.5 × 10 ⁻⁸	4.5 ± 0.1 × 10 ⁻⁴	12
 Viologen-based Polymer	5.2 mM / 0.1 M NaCl	7.6 ± 0.9 × 10 ⁻⁷	9 ± 2 × 10 ⁻⁵	12
P(FPMAm-co-METAC) (P2)	5 mM / 1 M NaCl	2.38 × 10 ⁻⁶	2.16 × 10 ⁻³	This work

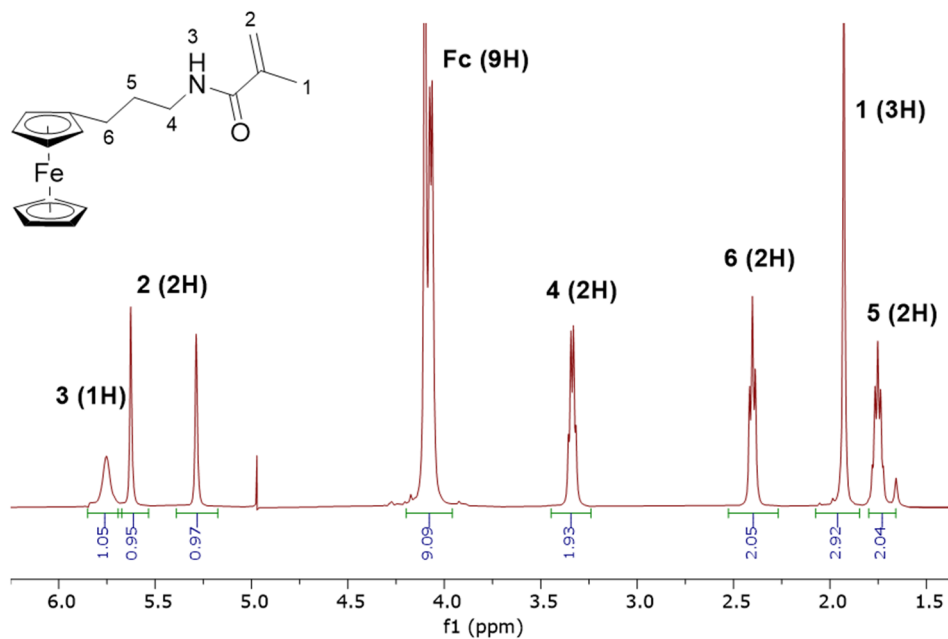


Figure S1. ¹H-NMR spectrum of 3-ferrocenylpropyl methacrylamide (FPMAm) (500 MHz, CDCl₃)

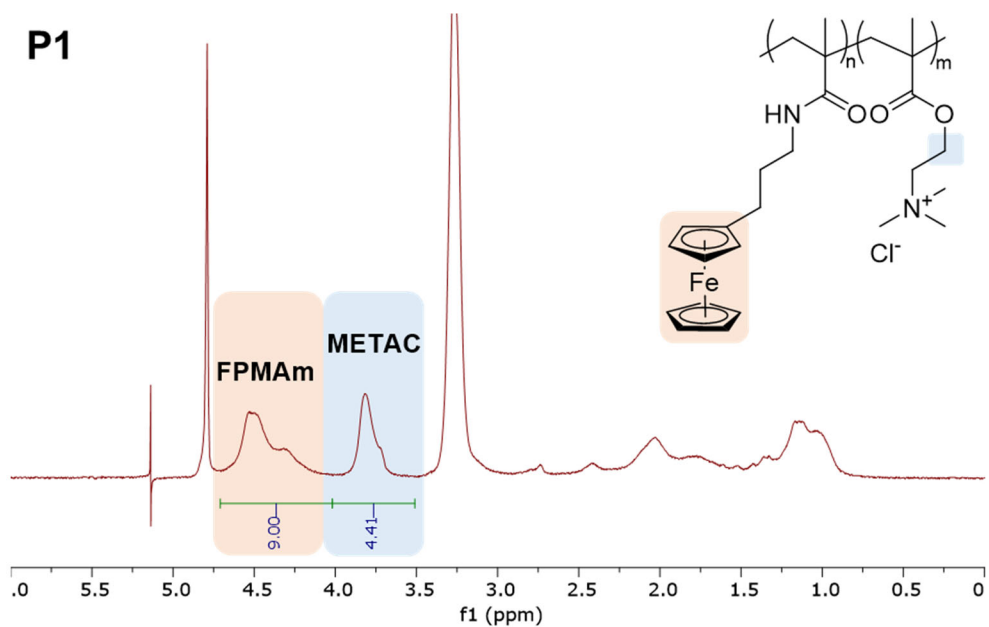


Figure S2. ¹H-NMR spectrum of P1 (P(FPMAm₃₁-co-METAC₆₉)) (500 MHz, D₂O)

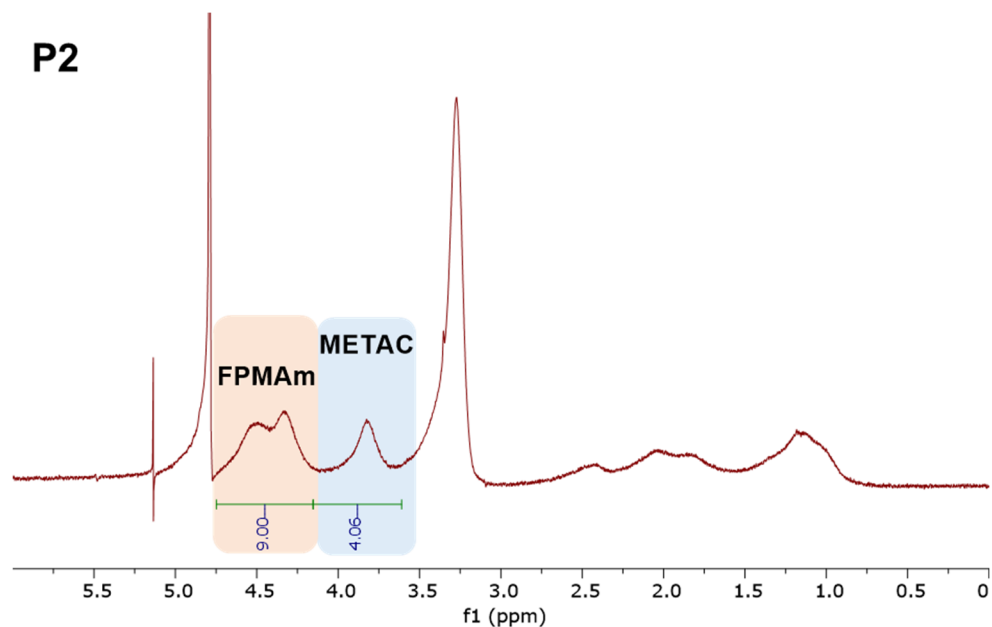


Figure S3. ¹H-NMR spectrum of P2 (P(FPMAm₃₃-co-METAC₆₇)) (500 MHz, D₂O)

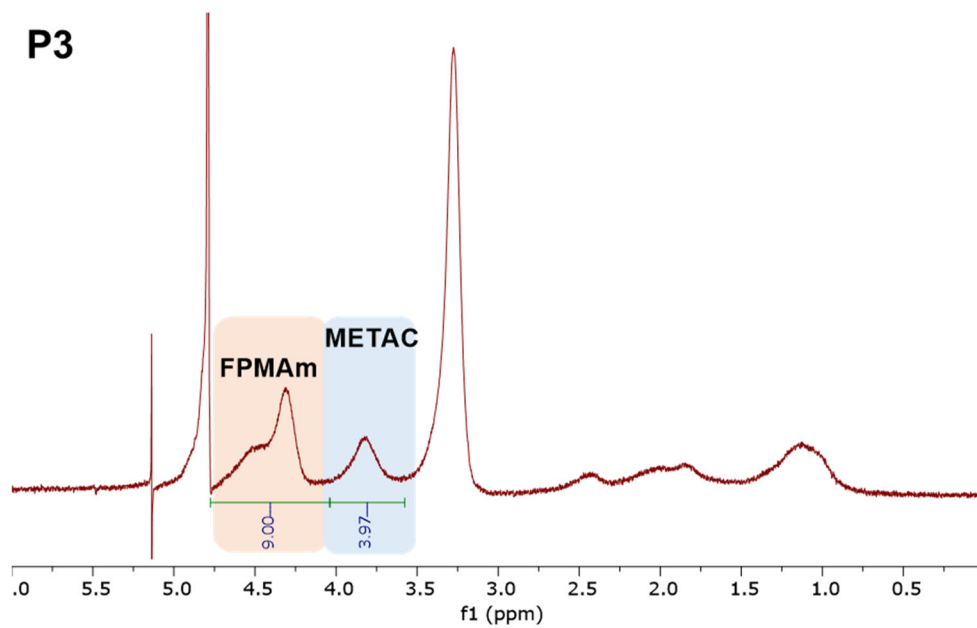


Figure S4. ¹H-NMR spectrum of P3 (P(FPMAm₃₄-co-METAC₆₆)) (500 MHz, D₂O)

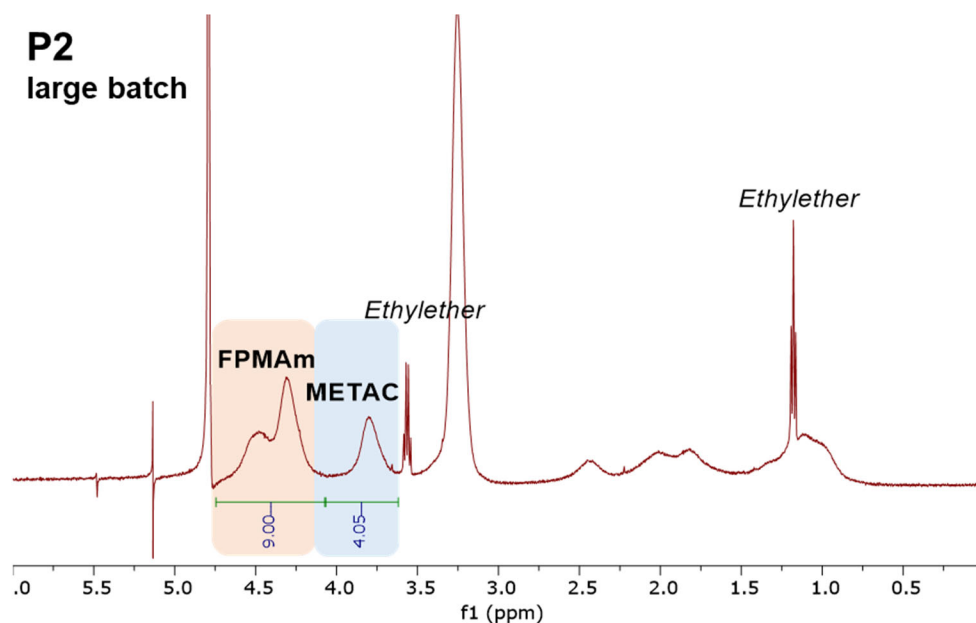


Figure S5. ¹H-NMR spectrum of P2 large batch (P(FPMAM₃₃-co-METAC₆₇)) (500 MHz, D₂O)

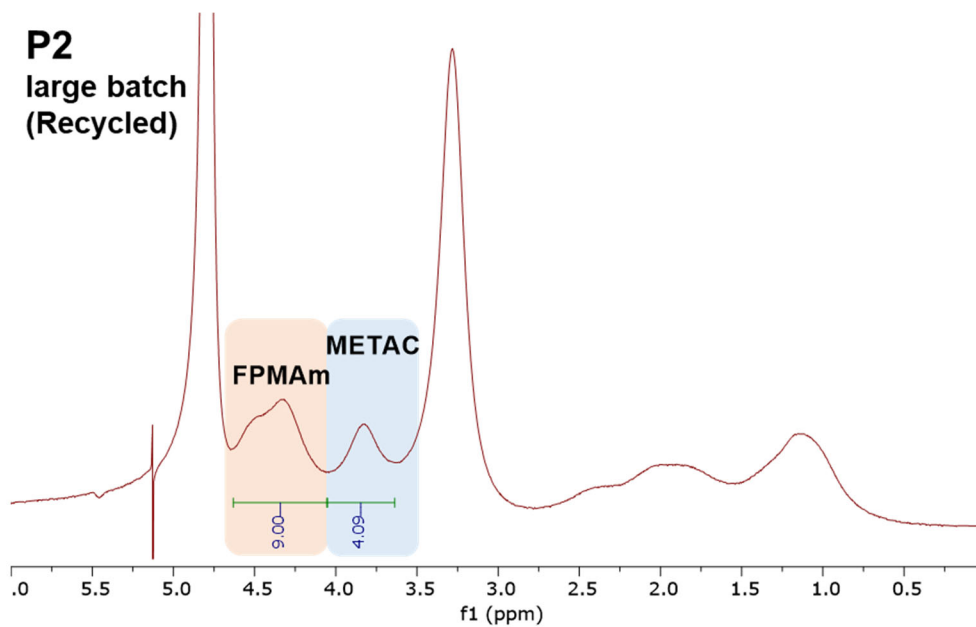


Figure S6. ¹H-NMR spectrum of P2 after recovery (P(FPMAM₃₃-co-METAC₆₇)) (500 MHz, D₂O). Note that the ratio between FPMAM and METAC does not change, indicating that the polymer is recyclable. We used recycled polymers for sequential experiments in this paper.

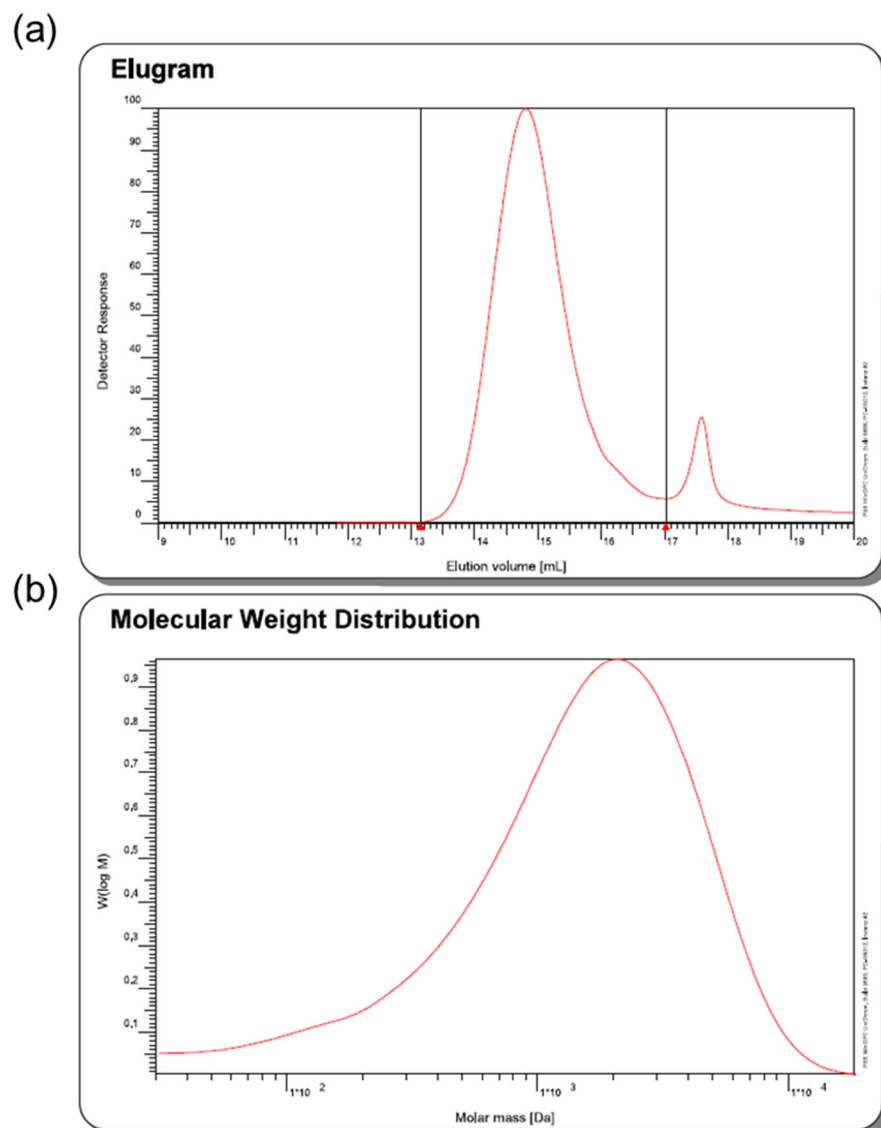


Figure S7. GPC results for P1: (a) Elugram and (b) molecular weight distribution. The curve was integrated from 13.15 mL to 17.02 mL. GPC was performed with respect to the poly(2-vinylpyridine) standard using the column of PSS NOVEMA Max in 0.1 M NaCl and 0.1 vol% TFA. The sample volume of 50 μ L was injected and ran the GPC with a flow rate of 1 mL/min.

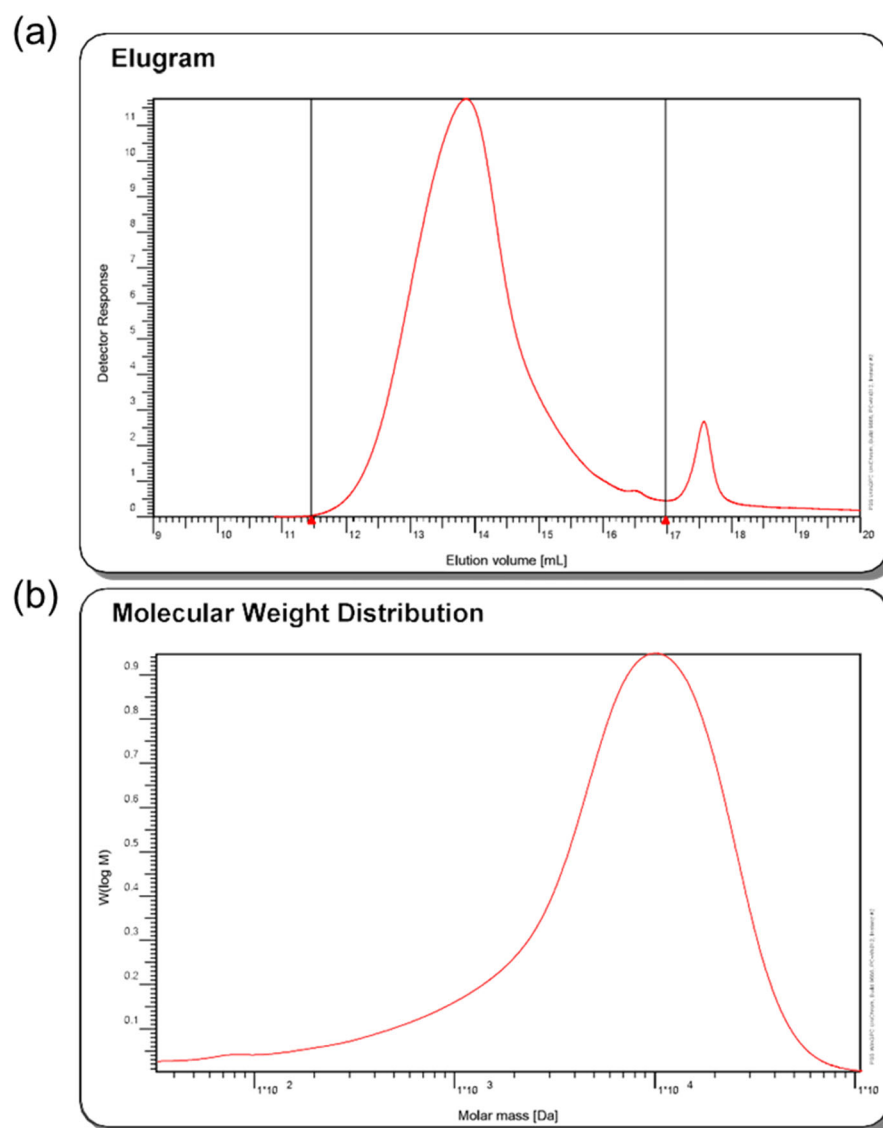


Figure S8. GPC results for P2: (a) Elugram and (b) molecular weight distribution. The curve was integrated from 11.46 mL to 16.98 mL. GPC was performed with respect to the poly(2-vinylpyridine) standard using the column of PSS NOVEMA Max in 0.1 M NaCl and 0.1 vol% TFA. The sample volume of 50 μ L was injected and ran the GPC with a flow rate of 1 mL/min.

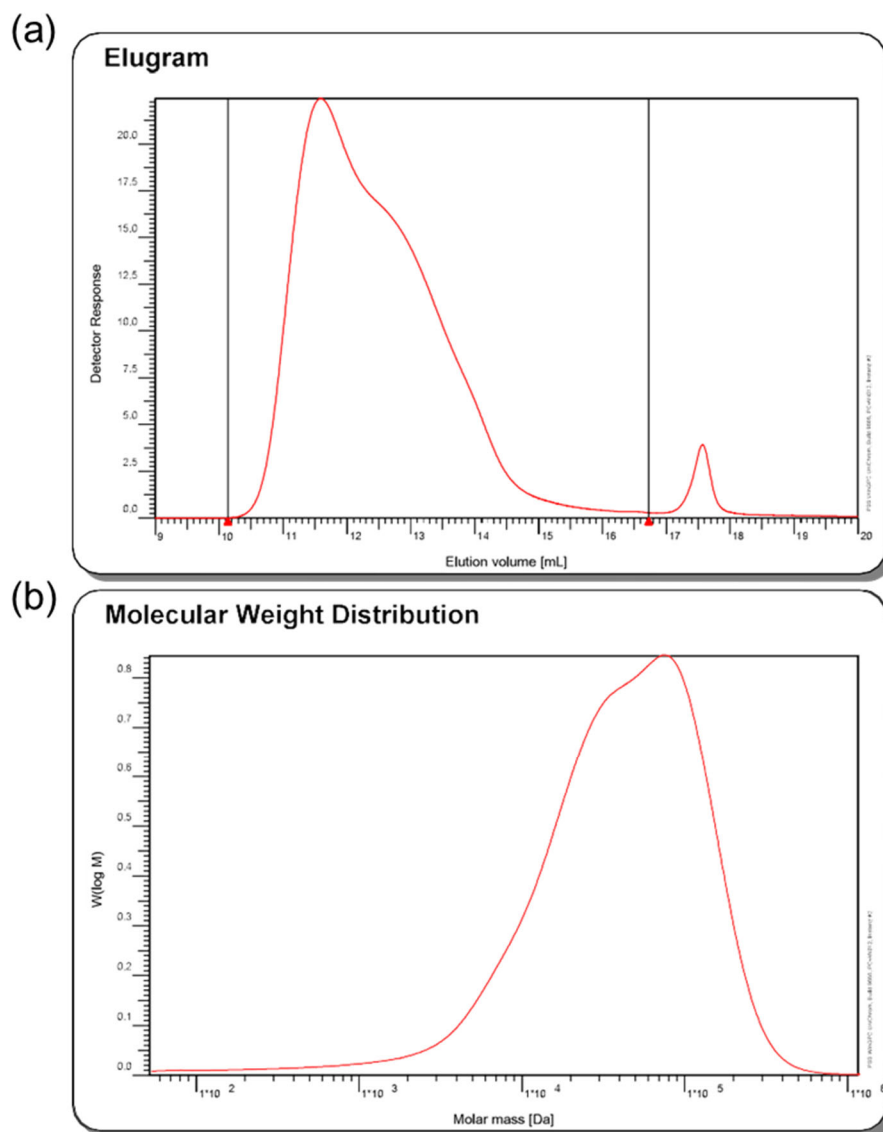


Figure S9. GPC results for P3: (a) Elugram and (b) molecular weight distribution. The curve was integrated from 10.14 mL to 16.73 mL. GPC was performed with respect to the poly(2-vinylpyridine) standard using the column of PSS NOVEMA Max in 0.1 M NaCl and 0.1 vol% TFA. The sample volume of 50 μ L was injected and ran the GPC with a flow rate of 1 mL/min.

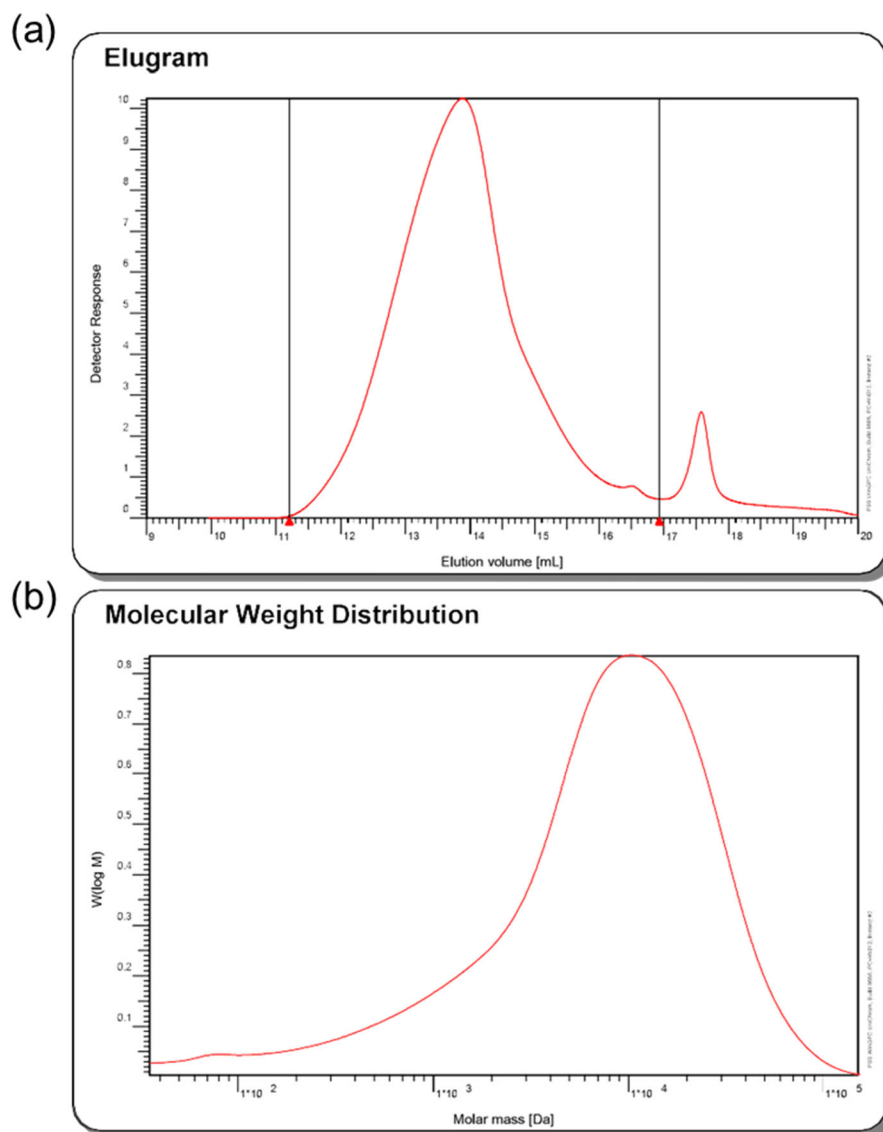


Figure S10. GPC results for P2 for large batch: (a) Elugram and (b) molecular weight distribution. The curve was integrated from 11.21 mL to 16.93 mL. GPC was performed with respect to the poly(2-vinylpyridine) standard using the column of PSS NOVEMA Max in 0.1 M NaCl and 0.1 vol% TFA. The sample volume of 50 μ L was injected and ran the GPC with a flow rate of 1 mL/min.

SI III. Electrochemical characterizations

Calculation of the diffusion coefficient and electron-transfer rate constant

With cyclic voltammetry and rotating disc electrode experiments, we calculated diffusion coefficient (D) and electron-transfer rate constant (k^0). For diffusion constant, we used the Randles-Sevcik equation for reversible systems:

$$i_p = 0.4463nFAC(nFvD/RT)^{0.5}$$

Assuming that the solution is at 25 °C, the equation can be simplified as follows:

$$i_p = 0.4463nFAC(nFvD/RT)^{0.5} = (2.687 \times 10^5)n^{3/2}ACD^{1/2}v^{1/2} \quad (\text{Equation 1})$$

, where i_p is the peak current (A), n is the number of electrons transferred in the redox reaction (in our polymer $n=1$), v is scan rate ($V s^{-1}$), D is the diffusion coefficient ($cm^2 s^{-1}$), C is the concentration of redox species ($mol cm^{-3}$), and A is the surface area of the working electrode (cm^2).

To calculate the electron-transfer rate constant, we used the Koutecky'-Levich equation to solve mass-transfer-independent current (known as kinetic current i_k):

$$1/i = 1/i_k + \frac{1}{0.62nFAD^{2/3}v^{1/6}C} \omega^{-1/2} \quad (\text{Equation 2})$$

, where i is current, F is Faraday's constant, v is the viscosity of redox material, and ω is rotation speed (rpm).

Plotting the inverse of current with respect to $\omega^{-1/2}$, the intercept is the inverse of kinetic current i_k . Then the kinetic current can be plotted in a Tafel plot ($\log|i_k|$ vs overpotential) to get the $i_k(0)$. Then based on the Butler-Volmer equation (Equation 3), the intercept of the Tafel plot ($i_k(0)$) can be used to calculate the k^0 as shown in Equation 4:

$$1/i_k = \exp(\eta F/RT)/2FAk^0C \quad (\text{Equation 3})$$

$$k^0 = \frac{i_k(0)}{AFC} \quad (\text{Equation 4})$$

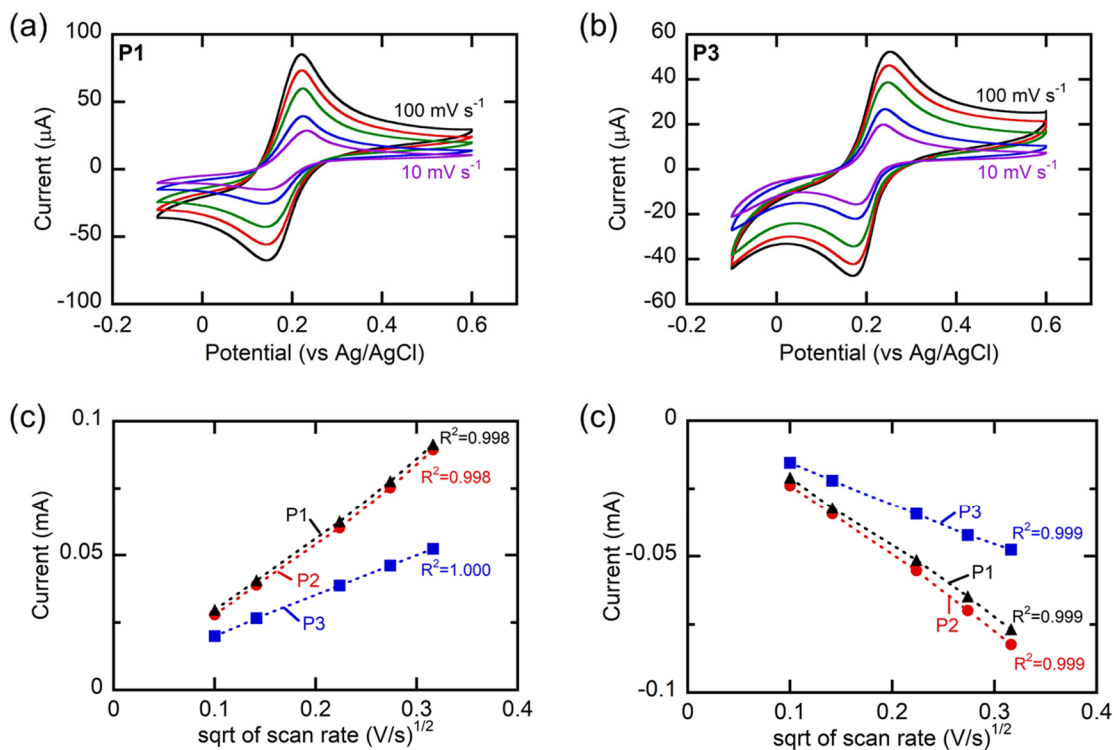


Figure S11. Cyclic voltammetry (CV) characterizations: (a, b) CV plots for P1 and P3 at varying scan rates (100, 75, 50, 20, 10 mV s^{-1}) and Randel Sevic plots (current vs. square root of scan rate) for (c) oxidation and (d) reduction currents. The CV measurements were conducted using 5 mM of redox-active substances (FPMAM contents) and 1 M NaCl with IR compensation. Pt wire was used as both working and counter electrodes, and Ag/AgCl (3M KCl) was used as a reference electrode.

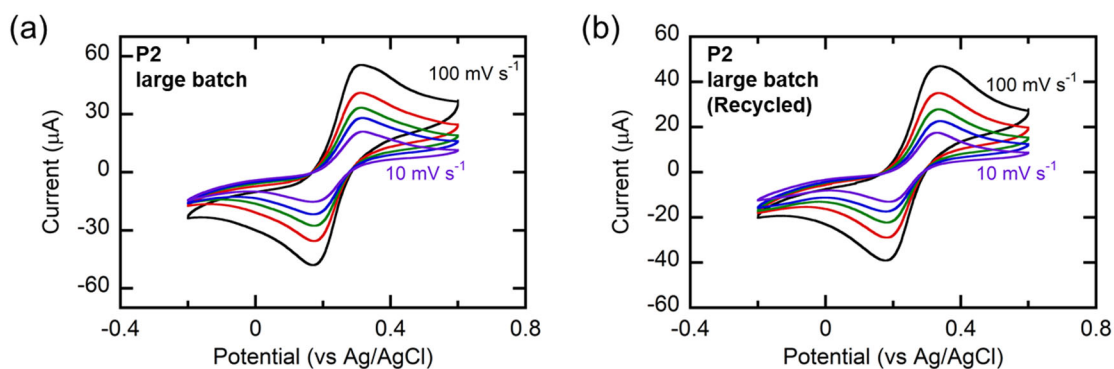


Figure S12. Cyclic voltammetry (CV) characterizations: (a) CV plots for P2 (large batch) (b) and recycled P2 (large batch). The CV measurements were conducted using 5 mM of redox-active substances (FPMAM contents) and 1 M NaCl with IR compensation. Pt wire was used as both working and counter electrodes, and Ag/AgCl (3M KCl) was used as a reference electrode.

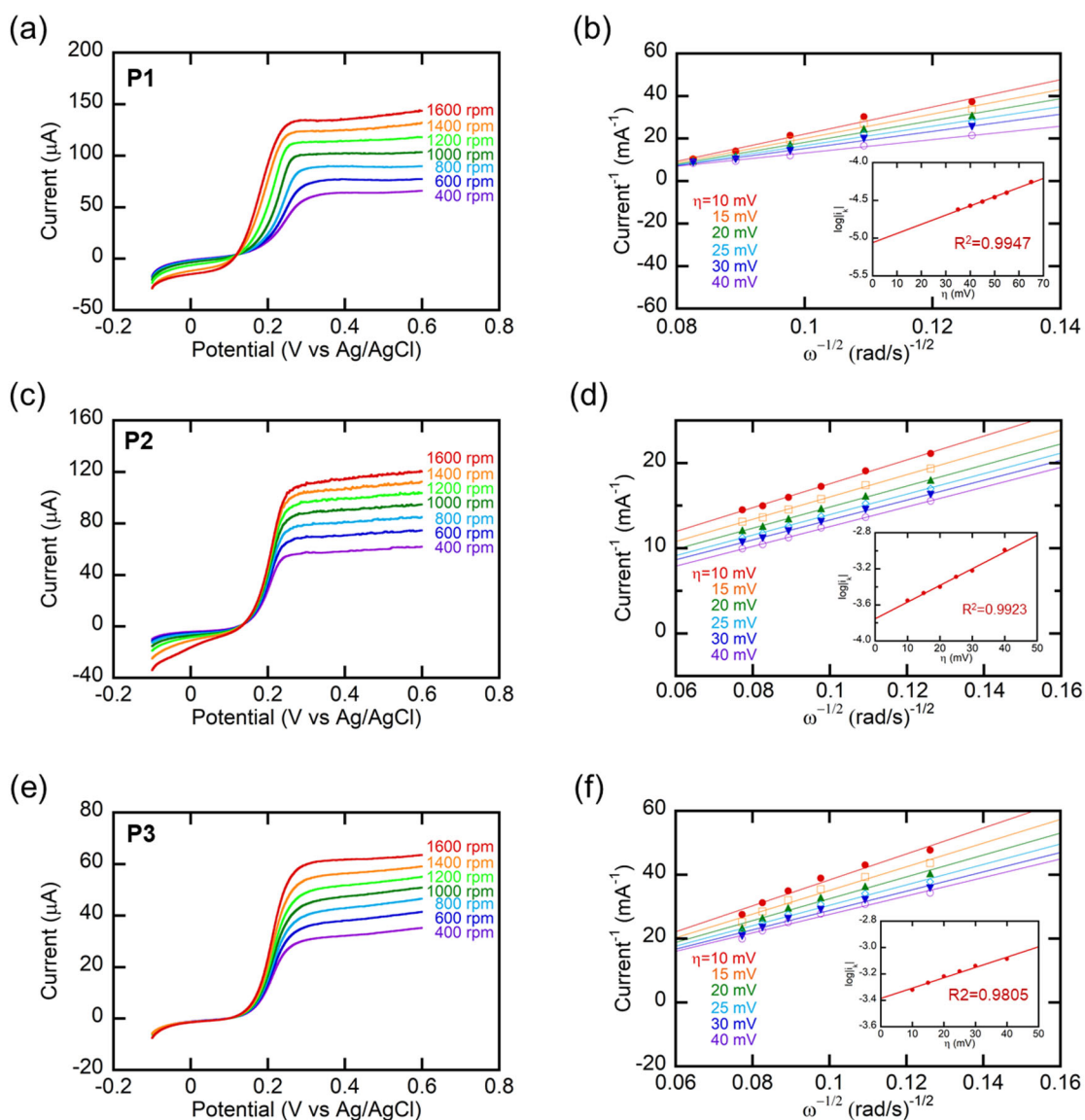


Figure S13. Rotating-disc electrode measurements: RDE measurements at rotating electrode speed between 400 and 1,600 rpm, Koutecky-Levich plots, and Tafel plots (inset) for (a,b) P1, (c,d) P2, and (e,f) P3. The measurements were performed at 5 mM of redox-active materials (FPMAm contents) and 1 M NaCl. Pt with a diameter of 5 mm was used as working, while the carbon rod with a diameter of 5 mm and Ag/AgCl (3M KCl) were used as counter and reference electrodes, respectively.

SI IV. Performance of redox-polymer ED

Evaluation of desalination performance

The desalination performance was analyzed by several electrochemical metrics such as salt removal and accumulation rate ($\text{mmol m}^{-2}\text{h}^{-1}$), energy consumption (kJ mol^{-1}), and charge efficiencies (%). The salt removal and accumulation rates were calculated from the continuous conductivity profiles using Equation 5 and Equation 6, respectively.

$$\text{Salt removal rate (mmol m}^{-2}\text{h}^{-1}) = \frac{\sum(C_0 - C_n)v\Delta t}{At_{tot}} \quad (\text{Equation 5})$$

$$\text{Salt accumulation rate (mmol m}^{-2}\text{h}^{-1}) = \frac{\sum(C_n - C_0)v\Delta t}{At_{tot}} \quad (\text{Equation 6})$$

, where the C_0 and C_n are initial and effluent concentrations (mM), v is the flow rate (5 mL/min), Δt is the measurement interval (5 s), A is the system active surface ($4 \text{ cm} \times 4 \text{ cm}$), and t_{tot} is total operating time (4 h).

Then, energy consumption (kJ mol^{-1}) and charge efficiencies (%) were evaluated by Equation 7 and Equation 8, respectively.

$$\text{Energy consumption (kJ mol}^{-1}) = \frac{V \int Idt}{\text{salt removal}} \quad (\text{Equation 7})$$

$$\text{Charge efficiency (\%)} = \frac{\text{Salt removal}}{(\int Idt/F)} \quad (\text{Equation 8})$$

, where *Salt removal* is the total amount of salt removed (numerator of Equation 5), I is the current of the system (A), and V is operating voltage (V).

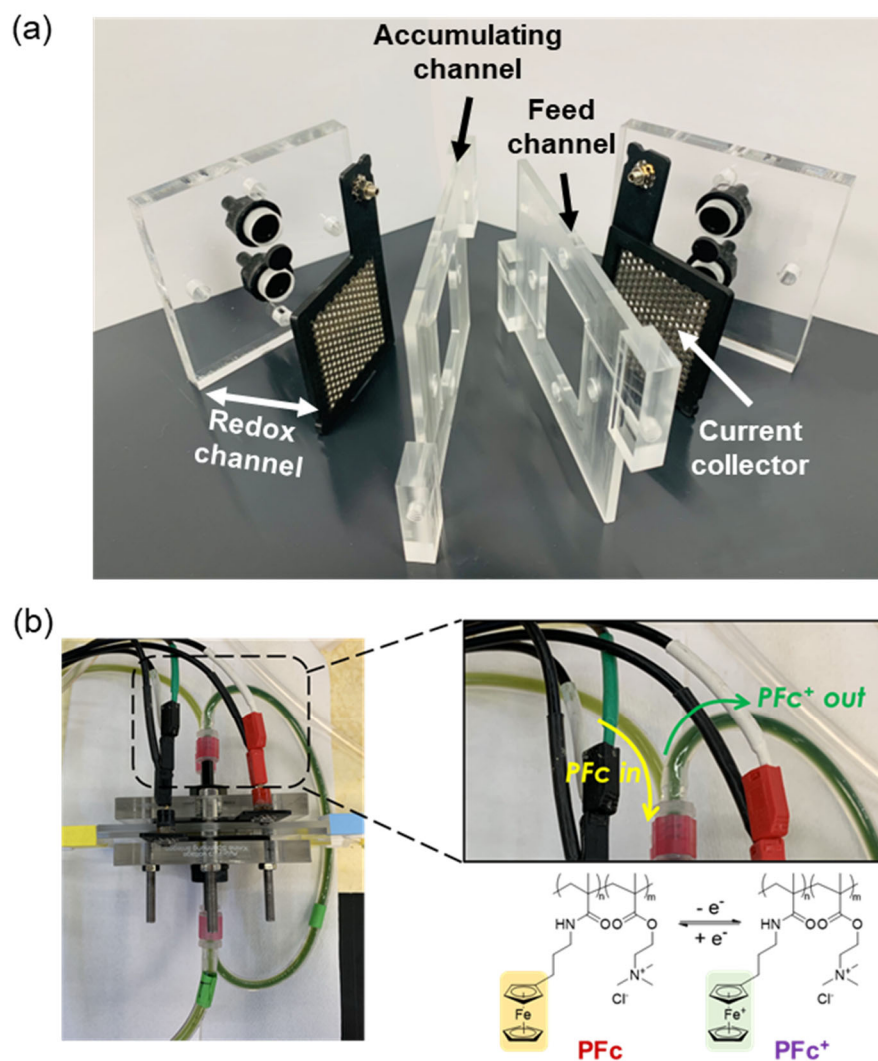


Figure S14. Redox-polymer ED system: (a) cell configurations and (b) simultaneous polymer redox reactions in the redox-polymer electrodiagnosis system. PFC and PFC⁺ represent reduced P(FPMAm-co-METAC) and oxidized P(FPMAm-co-METAC), respectively. As the redox-copolymer was continuously oxidized and reduced as it circulated the RC and revealed distinct colors between yellow (reduced) and green (oxidized).

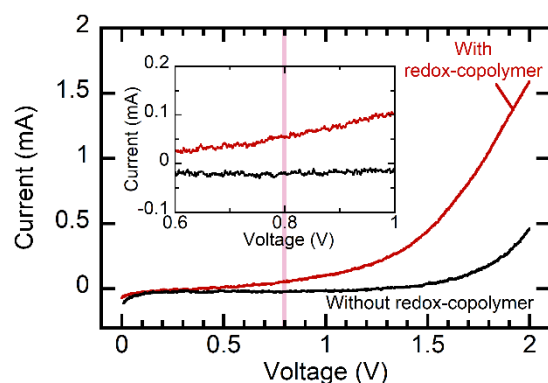


Figure S15. Linear sweep voltammetry (LSV) of the nanofiltration-enabled ED system in the presence of the redox-copolymer (the redox-polymer ED system) and in the absence of the redox-copolymer (the conventional ED system).

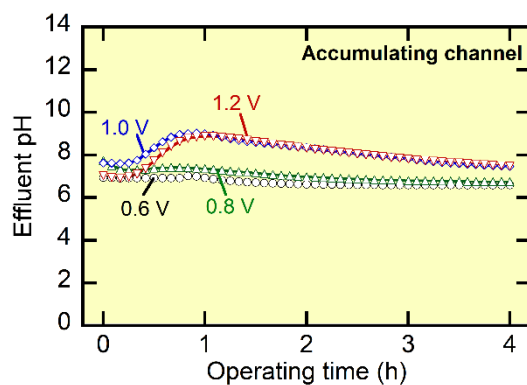


Figure S16. Desalination performance of the redox-polymer ED at varying operating voltages from 0.6 V to 1.2 V: (a) effluent pH in the accumulating channel. System was operated with a continuous flow of 10 mM NaCl in the FC and AC and 20 mL of 30 mM of the P(FPMAm-co-METAC) in the RC. For panels (a) and (b), black, green, blue, and red curves represent the operating voltage of 0.6, 0.8, 1.0, and 1.2 V, respectively.

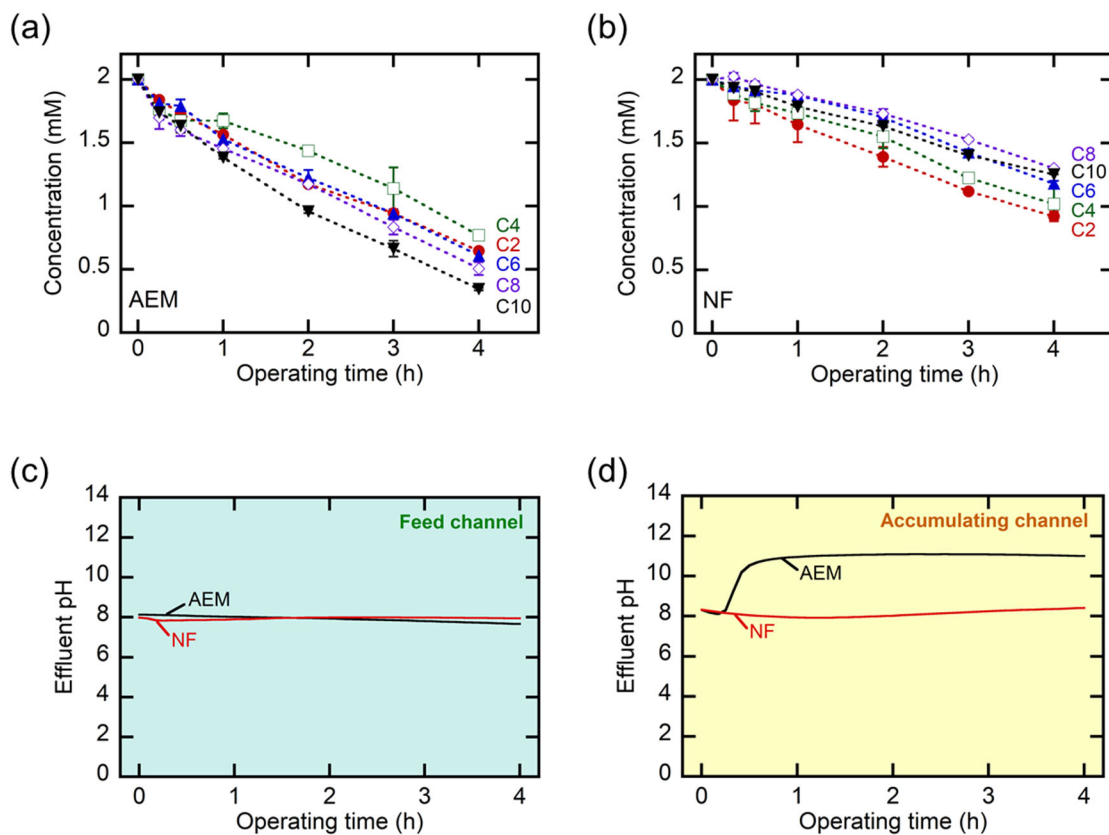


Figure S17. Concentration profile in the feed channel for carboxylate removal via (a) redox ED with AEMs and (b) the redox-polymer ED with NFs and effluent pH in the (c) feed channel and (d) accumulating channel. The experiment was performed with 50 mL of 2 mM of sodium acetate (C2), butyrate (C4), hexanoate (C6), octanoate (C8), and decanoate (C10) in the feed channel, while 50 mL of 10 mM NaCl was fed into the accumulating channel. The redox ED was performed with 20 mL of 30 mM of sodium ferrocyanide, while the redox-polymer ED was performed with 20 mL of 30 mM of P2.

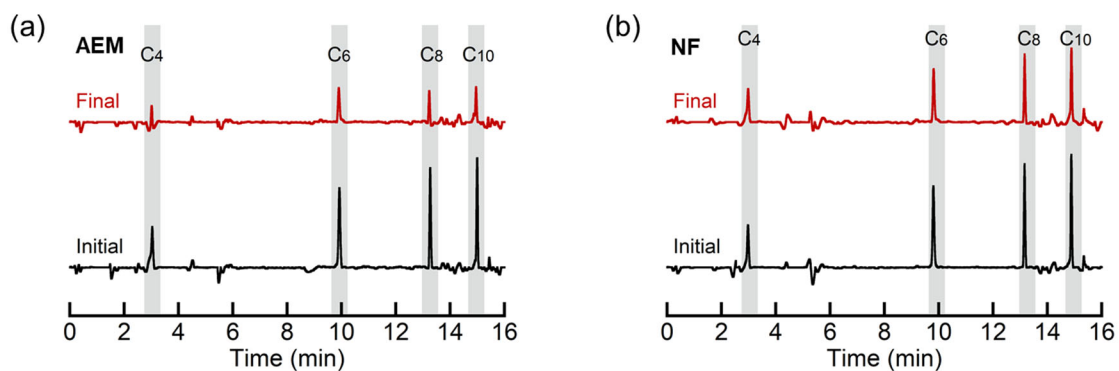


Figure S18. HPLC peak change for butyrate (C4), hexanoate (C6), Octanoate (C8), and decanoate (C10) in the FC via (a) redox ED with AEMs and (b) redox-polymer ED with NFs.

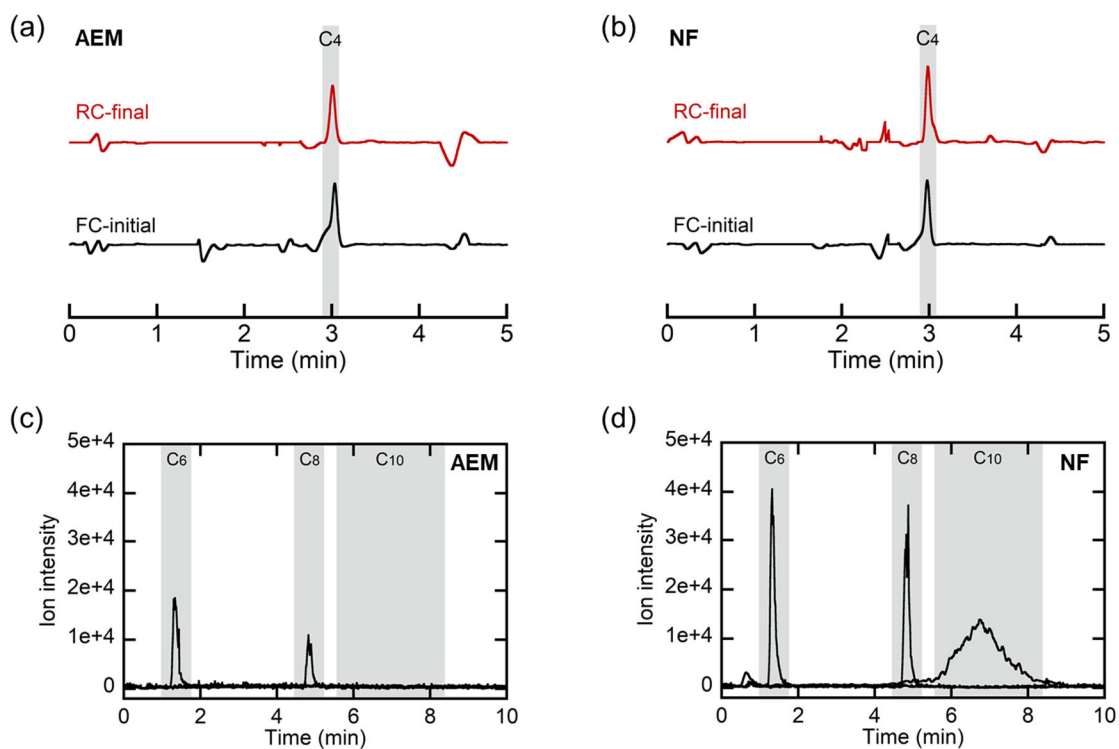


Figure S19. Reversible removal of carboxylates: HPLC peak for butyrate (C4) in the RC after the experiment via (a) redox ED with AEMs and (b) redox-polymer ED with NFs. LC-MS peak for hexanoate (C6), Octanoate (C8), and decanoate (C10) in the RC after the experiment via (c) redox ED with AEMs and (d) redox-polymer ED with NFs. Final concentrations of C6, C8, and C10 were analyzed by LC-MS due to the presence of overlapping peaks between redox species and carboxylates (C6-C10) in UV-vis spectrophotometry.

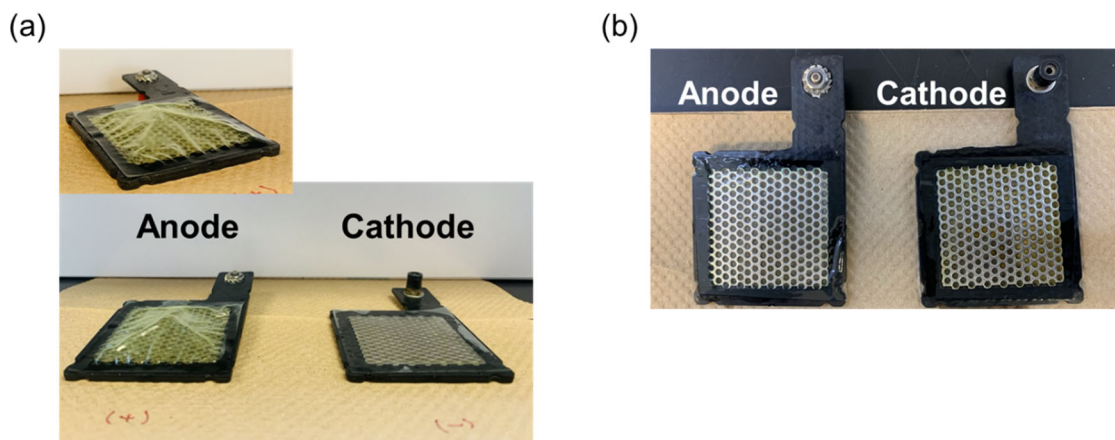


Figure S20. Fouling on the membrane in presence of carboxylates: membranes after electrochemical separation of carboxylates (between C2 and C10) via (a) redox ED with AEMs and (b) redox-polymer ED with NFs. For the redox ED with AEMs, the AEM between the anode and the FC has significant membrane swelling and noticeable color change compared to AEM on the cathode side and NFs.

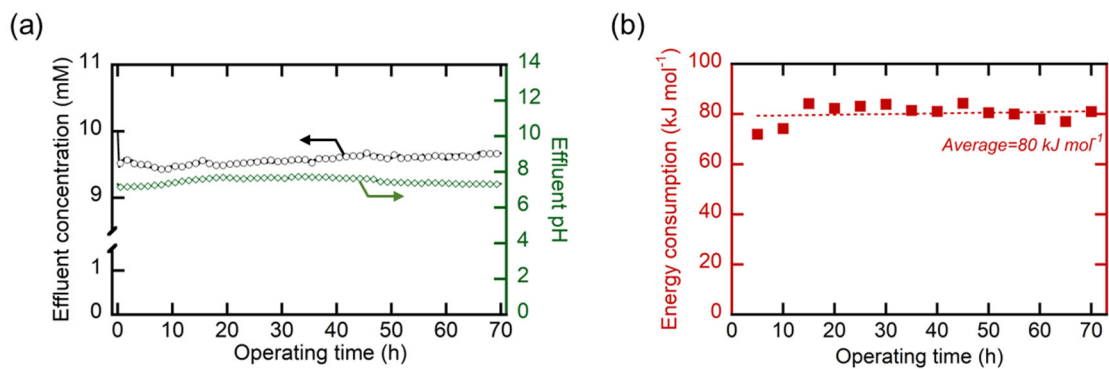


Figure S21. (a) Feed channel effluent concentration, pH, and (b) energy consumption over 70-hour desalination of the redox-polymer ED using recycled P(FPMAM-co-METAC). The system was operated with a continuous flow of 10 mM NaCl in the FC and AC and 20 mL of 30 mM of the P(FPMAM-co-METAC) in the RC.

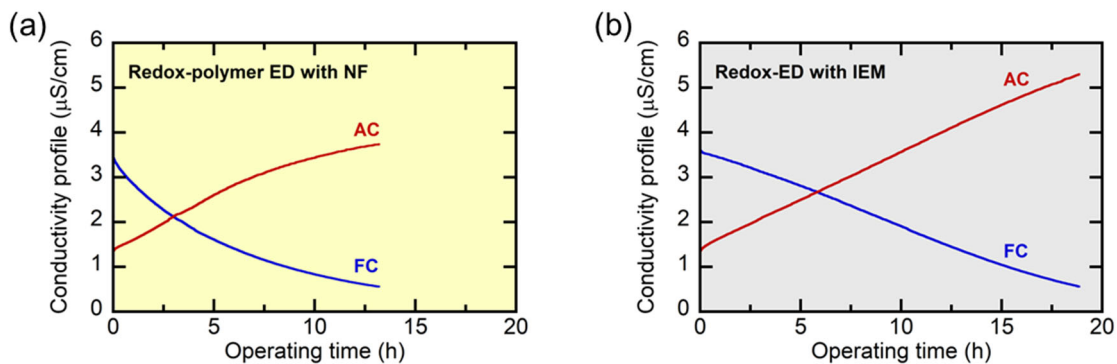


Figure S22. Conductivity profiles of (a) redox-polymer ED with NF and (b) redox-ED with IEM for treating wastewater down to potable water level, highlighting the fast kinetics of redox-polymer ED to perform desalination.

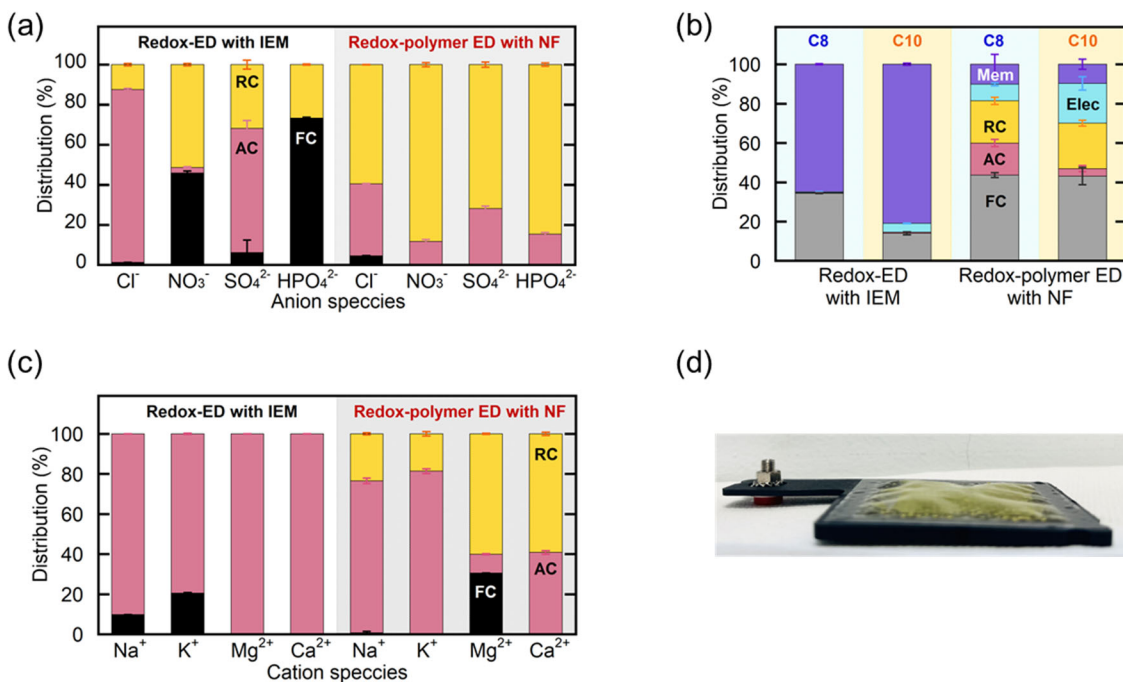


Figure S23. Distribution of (a) anion, (b) organic species, and (c) cation species after treating real wastewater and organic matters (C8 and C10) down to potable water level. (d) Physical deformation and irreversible adsorption of redox mediator (ferri-/ferrocyanide) on the anion-exchange membrane arranged between the anodic chamber and the FC after treating real wastewater and organic matters (C8 and C10) down to potable water level with the redox-ED system. Chloride distribution contains the initial concentration from wastewater and 10 mM Cl^- from the AC, while sodium distribution contains the initial concentration from wastewater and 10 mM Na^+ from the AC. In the case of redox-polymer ED, there is also an extra 55 mM of Cl^- from the counter-anion of P(FPMAm-co-METAC).

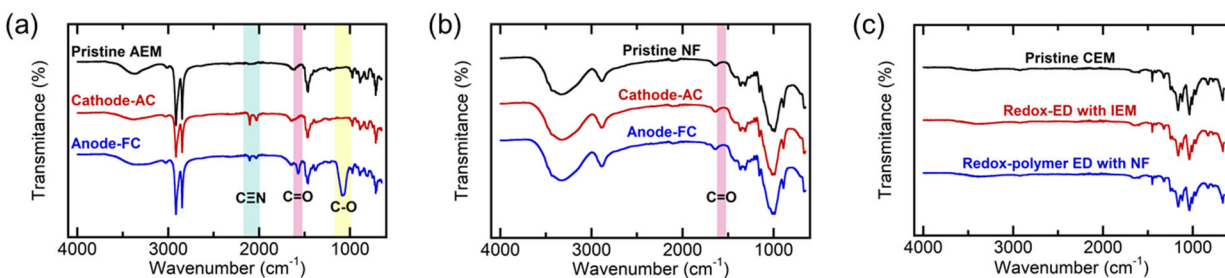


Figure S24. Fourier-transform infrared spectroscopy (FTIR) spectrum of NF, (b) AEM, and (c) CEM after wastewater treatment by redox-polymer ED with NF and redox-ED with IEM. Cathode-AC represents the membrane between the cathodic chamber and the accumulating channel, while anode-FC represents the membrane between the anodic chamber and the feed channel. CEM is arranged between the FC and AC for both systems.

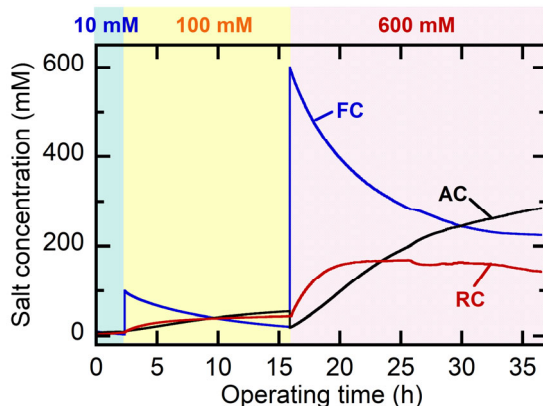


Figure S25. Concentration profiles for the FC, AC, and RC in series desalination of various source water (10-600 mM) without any additional treatment or system assembly. The desalination was conducted in a semi-continuous system with 20 mL of 30 mM P(FPMAm-co-METAC) in the RC, 20 mL of 10 mM NaCl in the AC, and 20 mL of treating water in the FC at the operating voltage of 0.8 V and the flow rate of 5 mL/min. A fraction of removed salts accumulated in the RC over time, and it reached equilibrated at around 150 mM. Based on the gradual increase/decrease of the salt concentrations in the AC/FC, the direction of ion migration was largely affected by the electric field. Although the back diffusion did not affect current sequential experiments, treating high-salinity source water down to potable water in a single cycle is challenging in the current state-of-art redox-polymer ED.

Table S4. The cation and anion composition of wastewater samples

Cation (mM)				Anion (mM)			
Na ⁺	K ⁺	Mg ²⁺	Ca ²⁺	Cl ⁻	NO ₃ ⁻	SO ₄ ²⁻	HPO ₄ ²⁻
26.5	1.79	2.38	0.343	16.14	1.16	6.99	0.116

Table S5. The concentration of Fe from the effluent in the feed and accumulating channels after a 4-hour operation at a varying concentration of P(FPMAM-co-METAC). The concentration of Fe was measured by the inductively coupled plasma-optical emission spectrometry (ICP-OES). ICP was operated with 2% HNO₃ as eluent with 10 times sample dilution. The detection limit of Fe is in ppb.

Concentration of PFPMAm (mM)	Concentration of Fe in the feed channel	Concentration of Fe in the accumulating channel
10	Not detected (ND)	ND
20	ND	ND
30	ND	ND
50	ND	ND

Table S6. The concentration of Fe from the effluent in the feed and accumulating channels after a 4-hour operation at a varying operating voltage. The concentration of Fe was measured by the inductively coupled plasma-optical emission spectrometry (ICP-OES). ICP was operated with 2% HNO₃ as eluent with 10 times sample dilution. The detection limit of Fe is in ppb.

Operating voltage (V)	Concentration of Fe in the feed channel	Concentration of Fe in the accumulating channel
0.6	Not detected (ND)	ND
0.8	ND	ND
1.0	ND	ND
1.2	ND	ND

Table S7. The concentration of Fe from the effluent in the feed and accumulating channels after a 4-hour operation at a varying electrolyte temperature. The concentration of Fe was measured by the inductively coupled plasma-optical emission spectrometry (ICP-OES). ICP was operated with 2% HNO₃ as eluent with 10 times sample dilution. The detection limit of Fe is in ppb.

Temperature at RC (°C)	Concentration of Fe in the feed channel	Concentration of Fe in the accumulating channel
5	Not detected (ND)	ND
RT (20-22)	ND	ND
40	ND	ND
60	ND	ND

Table S8. The concentration of Fe from the effluent in the feed and accumulating channels over a 70-hour operation (initial, 24, 48, 70 hours). The concentration of Fe was measured by the inductively coupled plasma-optical emission spectrometry (ICP-OES). ICP was operated with 2% HNO₃ as eluent with 10 times sample dilution. The detection limit of Fe is in ppb.

Time (h)	Concentration of Fe in the feed channel	Concentration of Fe in the accumulating channel
0	Not detected (ND)	ND
24	ND	ND
48	ND	ND
70	ND	ND

SI V. Techno-economic analysis

Mathematical models adopted in TEA

Mathematical approaches were referred mainly from the ED model developed by Generous et al.³ and McGovern et al.⁴ We evaluated TEA for redox-polymer ED and conventional ED with IEM (IEM ED). Both ED systems were assumed to be 1×1 m² size, and thus, the auxiliary equipment cost was assumed \$1,500.⁴ Also, since they 100 m³ per day for 330 days in a year, the labor cost for operating the system are equal (\$1,643 year⁻¹).³

Chemical cost (k_{ch}) of conventional ED (IEM ED), which is attributed to the cleaning, is calculated using Equation 9. For redox -polymer ED, a bulk amount of redox materials are taken into account of capital cost, and then annual chemical cost ($k_{ch,annual}$) can be calculated as Equation 10.

$$k_{ch} = 0.04 \times OD \times Q \quad (\text{Equation 9})$$

$$k_{ch,annual} = k_{ch} \times r + RED \times r \quad (\text{Equation 10})$$

, where 0.04 is unit chemical cost (\$ m⁻³), OD is operating days in a year (day), Q is feed flow rate per day (m³ day⁻¹), RED is the capital cost of redox material, and r is replacement cycle ($0 \leq r \leq 1$). We set the replacement cycle of the redox-copolymer to 0.5 considering that the redox-copolymer is recyclable.

The membrane cost is calculated based on the membrane unit price reported in the literature: 150 \$ m⁻² for ion-exchange membranes and 15 \$ m⁻² for nanofiltration membrane (cellulose-based membrane).^{4, 12-14} Then the total membrane cost is calculated by Equations 11 and 12 for the IEM ED and redox-polymer ED, respectively. Also, we assumed that the membrane replacement factor is 20%, implying that 20% of the membrane is replaced yearly ($0.2 \times k_m$).^{3, 15} Also, stacking cost is assumed to be 1.5 times the membrane cost (k_m).^{3, 15}

$$k_{IEM} = M_{IEM}(2n + 1) \quad (\text{Equation 11})$$

$$k_{NF} = M_{IEM}n + M_{NF}(n + 1) \quad (\text{Equation 12})$$

, where the M_{IEM} and M_{NF} are unit costs for IEM and NF, respectively and n is the number of the feed channel.

Stacking cost (k_{stack}) for the channel and electrodes are calculated based on the membrane, electrode, and current collector costs, which is modified from the calculation developed by Generous et al.³

$$k_{stack} = 0.5(k_{membrane} + k_{electrode} + k_{currentc collector}) \quad (\text{Equation 13})$$

Maintenance cost is estimated based on the capital cost (k_{cap}) as the following equations:³

$$k_{Maintenance} = 0.02k_{cap} \quad (\text{Equation 14})$$

Electricity is calculated with the following simplifications: i) both ED systems reveal comparable charge efficiencies and ii) they treat water continuously. Thus, iii) using LSV, we can estimate the operating voltages for IEM ED where the current is the same as the redox-polymer ED system operated at 0.8 V (**Figure S26**). With these simplifications, we can say that the cumulative charge for treating the equal amount of ions is the same, and the energy consumption is only dependent on the operating voltage. Then, the energy consumption per day can be computed by Equation 15.

$$E \text{ (kWh day}^{-1}\text{)} = V \int Idt / \textit{salt removal} \text{ (kJ/mol)} \times N_{NaCl} \times \frac{\textit{kWh}}{1000\textit{kJ}} \quad \text{(Equation 15)}$$

, where *salt removal* is the total salt removed in the 50 mM redox-polymer system at 0.8 V (0.635×10^{-3} mol), N_{NaCl} is the total amount of salt removed per day (580 mol day^{-1} based our assumption).

Using LSV and Equation 15, the daily energy consumption to treat 100 m^3 water with ED model is 13.5 and $25.6 \text{ kWh day}^{-1}$ for the redox-polymer ED and IEM ED, respectively. Then the yearly electricity cost can be determined based on the calculated energy consumption:

$$k_{\textit{electricity}} = 0.11 \times E \times OD \quad \text{(Equation 16)}$$

, where 0.11 is the average electricity cost in the United States ($\$ \text{ kWh}^{-1}$).

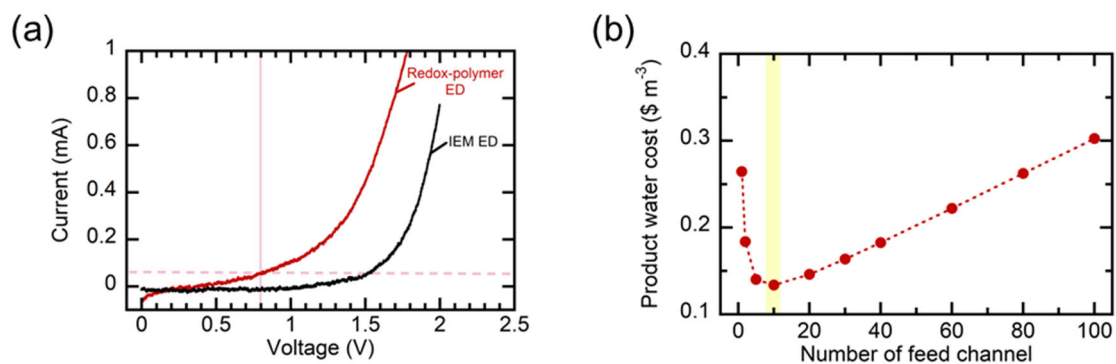


Figure S26. Evaluation and optimization of the techno-economic analysis: (a) linear sweep voltammetry for redox-polymer ED and IEM ED and (b) optimization of feed channel compartments for redox-polymer ED between the number of feed channels and the amount of redox material. For LSV, we used 50 mM of P(FPMAm-co-METAC), while 50 mM of NaCl was used for the IEM ED. The high solubility of P(FPMAm-co-METAC) (>1.0 M)¹⁶ enabled desalinating of a large volume of water with fewer feed channel stacks, and thus, reduced the total number of membranes than the conventional ED. Based on **Figure S22b**, we chose 10 feed channels and calculated the TEA as shown in **Table S10**.

Table S9. Techno-economic analysis for synthesis of P(FPMA_{m33}-co-METAC₆₇)

i) Cyanovinyl ferrocene synthesis									
Chemicals	MW	eq	mol	g	yield (%)	Price (\$)	Unit Price	Unit	Source
Ferrocene carboxaldehyde	214	1	0.6	139		17	120	\$/kg	a)
KOH	56.1	1	0.6	36		0.04	1	\$/kg	b)
Acetonitrile	41.1	82	53.3	2187		1	0.30	\$/kg	b)
2-Cyanovinyl ferrocene	237.08			146	95				
ii) Ferrocenyl propylamine synthesis									
Chemicals	MW	eq	mol	g	yield (%)	Price (\$)	Unit Price	Unit	Source
Cyanovinyl ferrocene	237	1	0.6	146					
Dihydrogen	2.02	3	1.9	4					
Raney nickel	58.7	1.2	0.7	43		0.22	5	\$/kg	b)
EtOH	46.1	40	24.7	1138		0.01	0.01	\$/kg	b)
NH ₄ OH	35.0	20	12.3	433		0.01	0.025	\$/kg	b)
3-Ferrocenyl propylamine	243.13			132	88				
iii) Ferrocenylpropylmethacrylamide synthesis									
Chemicals	MW	eq	mol	g	yield (%)	Price (\$)	Unit Price	Unit	Source
Ferrocenylpropylamine	243	1	0.5	132					
Methacrylic anhydride	154	1.2	0.7	101		0.01	0.1	\$/kg	b)
Triethylamine	101	1.2	0.7	66		0.131929	2	\$/kg	b)
Dichloromethane	84.93	60	32.6	2768		1.66	0.6	\$/kg	b)
FPMAm	311.21			110	65				
iv) Co-polymerization									
Chemicals	MW	Eq	mol	g	yield (%)	Price (\$)	Unit Price	Unit	Source
FPMAm	311	1	0.4	110					
METAC (28% water contents)	208	2.3	0.8	238		0.04	0.18	\$/kg	b)
ACVA	280	0.05	0.1	16		0.16	10	\$/kg	a)
MeOH	32.0	90	31.8	1018		0.28	0.278	\$/kg	b)
P(FPMA_{m33}-co-METAC₆₇)				100	91				
TOTAL Price (\$ per 100 g_{polymer})						20			
Unit price (\$ per g_{polymer})						0.20			

a).chemical book; b) alibaba

Table S10. The production cost of potable water for redox-polymer and conventional electro dialysis systems

	Redox-polymer ED	IEM ED	Unit Price	Unit	Ref/Source
Membrane (\$ system ⁻¹)	1,665	73,350	150 (IEM) 15 (NF)	\$ m ⁻²	12, 14
Chemical cost (\$ system ⁻¹)	1,320	1,320			
Redox materials (\$ system ⁻¹)	152	-	0.20	\$ g ⁻¹	-
Electrodes (\$ system ⁻¹)	976	-	20	\$ m ⁻²	
Current collector (\$ system ⁻¹)	244		5	\$ m ⁻²	17
Stack (\$ system ⁻¹)	1,442	36,675			3
Auxiliary equipment (\$ system ⁻¹)	1,500	1,500	1,500	\$ m ⁻²	4
Total capital cost (\$)	7,299	112,845			
Electricity (\$ yr ⁻¹)	491	930	0.11	\$ kWh ⁻¹	
Annual Chemical cost (\$ yr ⁻¹)	736	660			3
Membrane replacement (\$ yr ⁻¹)	333	14,670			3
Electrode replacement (\$ yr ⁻¹)	195				
Maintenance expenditure (\$ yr ⁻¹)	146	2257			3
Labor (\$ yr ⁻¹)	1,642	1,642	0.05	\$ m ⁻³	3
Total operating cost (\$ yr ⁻¹)	3,544	20,159			
Production cost (\$ m⁻³)	0.134	1.02			

References

- (1) Vapnik, H.; Elbert, J.; Su, X. Redox-copolymers for the recovery of rare earth elements by electrochemically regenerated ion-exchange. *Journal of Materials Chemistry A* **2021**, *9* (35), 20068-20077.
- (2) Kim, N.; Hong, S. P.; Lee, J.; Kim, C.; Yoon, J. High-desalination performance via redox couple reaction in the multichannel capacitive deionization system. *ACS Sustainable Chemistry & Engineering* **2019**, *7* (19), 16182-16189. Kim, N.; Jeon, J.; Elbert, J.; Kim, C.; Su, X. Redox-mediated electrochemical desalination for waste valorization in dairy production. *Chemical Engineering Journal* **2022**, *428*, 131082.
- (3) Generous, M. M.; Qasem, N. A.; Akbar, U. A.; Zubair, S. M. Techno-economic assessment of electrodialysis and reverse osmosis desalination plants. *Separation and Purification Technology* **2021**, *272*, 118875.
- (4) McGovern, R. K.; Weiner, A. M.; Sun, L.; Chambers, C. G.; Zubair, S. M. On the cost of electrodialysis for the desalination of high salinity feeds. *Applied Energy* **2014**, *136*, 649-661.
- (5) Sajtar, E. T.; Bagley, D. M. Electrodialysis reversal: Process and cost approximations for treating coal-bed methane waters. *Desalination and Water Treatment* **2009**, *2* (1-3), 284-294.
- (6) Yamamura, T.; Watanabe, N.; Yano, T.; Shiokawa, Y. Electron-transfer kinetics of $\text{Np}^{3+}/\text{Np}^{4+}$, $\text{NpO}_2^{2+}/\text{NpO}_2$, $\text{V}^{2+}/\text{V}^{3+}$, and $\text{VO}_2^{+}/\text{VO}_2$ at carbon electrodes. *Journal of The Electrochemical Society* **2005**, *152* (4), A830.
- (7) Konopka, S.; McDuffie, B. Diffusion coefficients of ferri- and ferrocyanide ions in aqueous media, using twin-electrode thin-layer electrochemistry. *Analytical Chemistry* **1970**, *42* (14), 1741-1746.
- (8) Daum, P. H.; Enke, C. G. Electrochemical kinetics of the ferri-ferrocyanide couple on platinum. *Analytical Chemistry* **1969**, *41* (4), 653-656.
- (9) Beh, E. S.; De Porcellinis, D.; Gracia, R. L.; Xia, K. T.; Gordon, R. G.; Aziz, M. J. A neutral pH aqueous organic-organometallic redox flow battery with extremely high capacity retention. *ACS Energy Letters* **2017**, *2* (3), 639-644.
- (10) Hu, B.; DeBruler, C.; Rhodes, Z.; Liu, T. L. Long-cycling aqueous organic redox flow battery (AORFB) toward sustainable and safe energy storage. *Journal of the American Chemical Society* **2017**, *139* (3), 1207-1214.
- (11) Zhou, W.; Liu, W.; Qin, M.; Chen, Z.; Xu, J.; Cao, J.; Li, J. Fundamental properties of TEMPO-based catholytes for aqueous redox flow batteries: Effects of substituent groups and electrolytes on electrochemical properties, solubilities and battery performance. *RSC Advances* **2020**, *10* (37), 21839-21844.
- (12) Janoschka, T.; Martin, N.; Martin, U.; Friebe, C.; Morgenstern, S.; Hiller, H.; Hager, M. D.; Schubert, U. S. An aqueous, polymer-based redox-flow battery using non-corrosive, safe, and low-cost materials. *Nature* **2015**, *527* (7576), 78-81.
- (13) Yan, W.; Wang, C.; Tian, J.; Zhu, G.; Ma, L.; Wang, Y.; Chen, R.; Hu, Y.; Wang, L.; Chen, T. All-polymer particulate slurry batteries. *Nature communications* **2019**, *10* (1), 1-11.
- (14) Lee, H.-J.; Sarfert, F.; Strathmann, H.; Moon, S.-H. Designing of an electrodialysis desalination plant. *Desalination* **2002**, *142* (3), 267-286.
- (15) Strathmann, H. *Ion-exchange membrane separation processes*; Elsevier, 2004.
- (16) Borchers, P. S.; Strumpf, M.; Friebe, C.; Nischang, I.; Hager, M. D.; Elbert, J.; Schubert, U. S. Aqueous Redox Flow Battery Suitable for High Temperature Applications Based on a Tailor-Made Ferrocene Copolymer. *Advanced Energy Materials* **2020**, *10* (41), 2001825.
- (17) Hand, S.; Guest, J. S.; Cusick, R. D. Technoeconomic analysis of brackish water capacitive deionization: navigating tradeoffs between performance, lifetime, and material costs. *Environmental science & technology* **2019**, *53* (22), 13353-13363.